JCTC Journal of Chemical Theory and Computation

Theory of High-Spin d^4 Complexes: An Angular-Overlap Model Parametrization of the Ligand Field in Vibronic-Coupling Calculations

Graham Carver,[†] Markus Thut,[‡] Christopher Noble,[§] and Philip L. W. Tregenna-Piggott*,[†]

Laboratory for Neutron Scattering, PSI, CH-5232 Villigen, Switzerland, Department of Chemistry and Biochemistry, University of Bern, Freiestrasse 3, CH-3012 Bern, Switzerland, and Centre for Magnetic Resonance, The University of Queensland, Brisbane, Australia

Received December 22, 2007

Abstract: A new theoretical approach for the calculation of the electronic and molecular structures of octahedrally-coordinated high-spin d^4 complexes is described. A prescription for the construction of an effective $^3T_1 + {}^5E$ (O) Hamiltonian from the ligand-field matrices of a complex with general trigonal symmetry is given, where the ligand field is parametrized in terms of the angular-overlap model (AOM). The Jahn–Teller matrices for the $^3T_1 + ({}^5E\otimes e)$ vibronic Hamiltonian are constructed and the lowest eigenvalues are calculated by a numerical method. The model obviates the need to assume a temperature dependence of bonding parameters, inherent to the conventional ligand-field-theory approach and is applicable over the whole range of vibronic-coupling strengths, as demonstrated by example calculations on the $[Mn(OD_2)_6]^{3+}$ cation and $MgO:Cr^{2+}$.

1. Introduction

The resurgence of interest in the theoretical description of non-Kramers ions is undoubtedly due to the advent of the high-field EPR (HFEPR) technique. Oxidative stability, topicality, and the sheer fact that they invariably yield good spectra have all contributed to compounds of Mn(III) emerging as the deliciae of HFEPR spectroscopists. The strong Jahn–Teller effect, inherent to complexes of Mn(III), is usually incorporated into the analyses, only insofar as it leads to a tetragonally-distorted geometry. Dynamical Jahn–Teller coupling, which affects both the electronic and molecular structures of high-spin d^4 complexes, is usually ignored. This work describes a theoretical approach to calculating the electronic and molecular structures of octahedral high-spin d^4 complexes, which combines the chemically intuitive angular-overlap model with the rigor of vibronic-coupling calculations.

This work follows on from a recent article, in which crystallographic and spectroscopic data were presented for the $[Cr(OD_2)_6]^{2+}$ cation in the Cr(II) Tutton's salt and modeled using a $^5E\otimes e$ vibronic-coupling Hamiltonian.[1] The calculations provided a good account of the available spectroscopic and structural data and aptly demonstrated the need for a theoretical approach that goes beyond the conventional ligand-field model to include the vibrational coordinates of the molecule. The model is limited in its application, however, as the matrix elements of the spin–orbit interaction in the effective ^5E (O) electronic matrix were derived by perturbation theory, assuming perfect cubic symmetry in the strong-ligand-field limit. Even in cases of exact cubic symmetry, this model can serve only as a guide as to the magnitude of the spin–orbit splitting of the ^5E term. For this reason, the discussion focused on an interpretation of the ratio of the axial and rhombic zero-field-splitting parameters, D and E, as a function of temperature, rather than their absolute values.

For octahedral Mn(III) complexes, this approach is wholly inappropriate for two reasons. First, the ratios of the

* E-mail: philip.tregenna@psi.ch.
[†] Laboratory for Neutron Scattering.
[‡] University of Bern.
[§] The University of Queensland.

10.1021/ct7003484 CCC: $40.75
Published on Web 03/18/2008

octahedral-splitting parameter, 10Dq to the Racah parameters, B and C, for a Mn(III) complex are larger than for the corresponding Cr(II) complex. Hence, the difference in the energies of the ^5E and excited $^3T_1$ terms will be much reduced, being comparable in magnitude to the spin–orbit-coupling parameter, ζ. In this case the effect of the spin–orbit-coupling matrix elements between these terms, which largely governs the ground-state spin-Hamiltonian parameters, can no longer be treated as a perturbation. Second, for octahedrally coordinated Mn(III) complexes the ground-state zero-field splitting is far more susceptible to the trigonal component of the ligand field.[2]

In order for vibronic-coupling calculations of Mn(III) complexes to be meaningful, the effective electronic Hamiltonian must therefore be generated in the point group of the undistorted complex and off-diagonal spin–orbit-coupling matrix elements between the ^5E and excited $^3T_1$ terms must be included explicitly. This article presents a procedure for calculating the effective electronic Hamiltonian spanning the basis functions of the $^3T_1$ and ^5E terms, using ligand-field matrices generated by the angular-overlap model (AOM). Calculations of the ground-state electronic and low-temperature molecular structures of $MgO:Cr^{2+}$ and the $[Mn(OD_2)_6]^{3+}$ cation in the cesium manganese alum, using the $^3T_1 + (^5E\otimes e)$ vibronic Hamiltonian serve to illustrate the model's wide applicability. The dependence of the electronic and molecular structures on the parameters of the vibronic Hamiltonian is discussed in the light of existing theoretical models.

2. Review of Previous Models

In the following sections, we summarize the various approaches that have been applied to model experimental data obtained for high-spin d^4 complexes.

2.1. Ligand-Field Theory. The ground-state energies and geometries of high-spin d^4 transition-metal complexes are frequently rationalized in terms of a ligand-field or crystal-field model.[3,4] The ^5D free-ion ground term is split through a cubic field, giving rise to a ^5E_g (O_h) ground term and a higher-lying $^5T_{2g}$ term. In the ligand-field description the ground term is split further by a tetragonal component of the ligand field, resulting in either a $^5A_{1g}$ or $^5B_{1g}$ (D_{4h}) term lower lying. Off-diagonal spin–orbit-coupling matrix elements between the ground singlet and higher-lying terms result in a zero-field splitting (zfs) of the orbital singlet. The resulting ground-state energy scheme is usually well described by the spin Hamiltonian,

$$H = D\left[S_z^2 - \frac{1}{3}S(S+1)\right] + E[S_x^2 - S_y^2] \qquad (1)$$

correct to second order, operating in the basis of the $S = 2$ spin functions, where D and E are the axial and rhombic zfs parameters, respectively.[5]

In symmetries lower than O_h there are matrix elements of spin–orbit coupling within the ^5E ground term. However, the dominant contributions to the zfs of the orbital-singlet ground term are the off-diagonal spin–orbit-coupling matrix elements between the ^5E_g and excited $^3T_{1g}$ and $^5T_{2g}$ (O_h) electronic terms. The following approximate expression for the axial zfs parameter, D has been derived by perturbation theory,[6]

$$D = \pm\left(\frac{\zeta^2}{6B + 5C - 10\mathrm{Dq}}\right) \pm \frac{3}{16}\left(\frac{\zeta^2}{10\mathrm{Dq}}\right) \qquad (2)$$

where B and C are the Racah parameters and 10Dq and ζ are the octahedral-splitting and spin–orbit-coupling parameters, respectively. The two contributions to D given here are those originating from the $^3T_{1g}$ and $^5T_{2g}$ terms, respectively; the upper sign holds for the $^5A_{1g}$ (D_{4h}) term lower lying, and the lower, for $^5B_{1g}$ lower lying. If the $^5B_{1g}$ term is lower lying, D is negative and the molecule has an elongated D_{4h} geometry. On the other hand, if the sign of the tetragonal field is reversed and the $^5A_{1g}$ term is lower lying, D is positive and the molecule has a compressed D_{4h} geometry.

Slight deviations of the symmetry of the ML_6 framework away from perfect D_{4h} symmetry correspond to an additional rhombic component in the crystal field and give rise to a nonzero rhombic zfs parameter. In the case of the $[Mn(OH_2)_6]^{3+}$ cation in the cesium manganese alum, where the rhombic distortion of the σ-bonding framework is barely significant, it has been demonstrated that the magnitude of the rhombic zfs parameter is governed by the strength and nature of the π-anisotropy of the surrounding ligands,[2] imposing a large trigonal ligand field.

The low-level energy schemes and associated molecular geometries of the majority of octahedral high-spin Mn(III) complexes can be rationalized in terms of ligand-field theory. Most hexa-coordinate homoleptic Mn(III) complexes with oxygen or nitrogen donors exhibit a tetragonally elongated geometry with a negative D.[2–4,7–9] In the comparatively few studies of octahedral Cr(II) complexes, a negative D with tetragonal elongation is also observed.[10] Interestingly, while a negative D was recently reported for the tetragonally-elongated γ-$Mn(acac)_3$ complex,[4] powder-magnetic-susceptibility studies by Gregson et al. performed on the tetragonally-compressed β-modification indicate a positive D value,[11] also in accordance with ligand-field theory.

By contrast, in the case of *trans*-$[Mn(cyclam)I_2]I$, despite a tetragonal elongation a positive D value is nonetheless observed.[12] The low-energy excitations in this complex are no longer of d−d character, and the observations are explained by considering interactions of the ground term with the low-energy LMCT terms; hence, in this instance, the ligand-field predictions are no longer valid.

2.2. Jahn–Teller Coupling. In instances of near or actual orbital degeneracy, high-spin d^4 complexes can exhibit a marked variation in the ligand-field parameters and bond lengths as a function of temperature, which cannot be explained within the framework of a "static" ligand-field model. A more rigorous approach allows for coupling of the electronic states to lattice vibrations via the Jahn–Teller interaction.

The Jahn–Teller effect is based on a theorem first described by Jahn and Teller in 1937,[13] following an original suggestion by Landau.[14] This theorem affirms that, in a nonlinear molecule having an electronically degenerate state (excepting

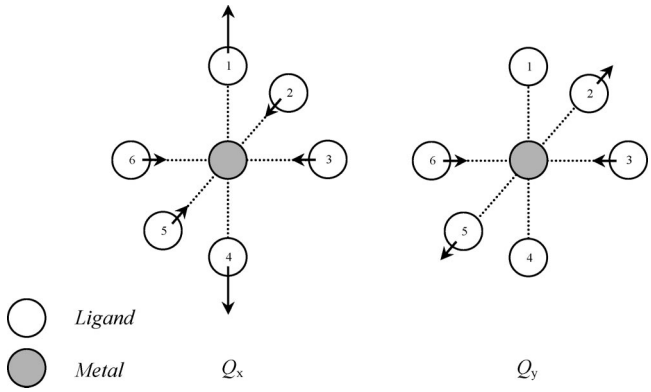

Figure 1. The two components of the $\nu_2(ML_6)$ vibration. Arrows indicate the directions and relative magnitudes of the displacements.

odd-electron systems having simple Kramers degeneracy), the nuclei of the molecule will displace themselves in order to destroy the symmetry of their configuration and to remove the electronic degeneracy. The Jahn–Teller effect cannot, however, reduce the overall degeneracy of a level, since the overall Hamiltonian retains its symmetry and remains totally symmetric under the operations of the point group of the system. The consequence of the Jahn–Teller interaction is thus to replace the original electronic degeneracy by vibronic degeneracy. Accordingly, the E⊗e Jahn–Teller interaction, operating within a ^{5}E electronic ground term will give rise to a vibronic-energy-level structure characterized by a ^{5}E vibronic ground term.

A Hamiltonian including both ligand-field and vibronic contributions has the general form,

$$H = H_{el} + H_{ph} + H_{JT} \tag{3}$$

where H_{ph} and H_{JT} are the phonon- and Jahn–Teller-coupling terms, respectively. H_{el} is the electronic part of the Hamiltonian given by

$$H_{el} = H_{ER} + H_{LF} + H_{SO} + H_{st} \tag{4}$$

where H_{ER}, H_{LF}, H_{SO}, and H_{st} designate the electron-repulsion, high-symmetry ligand-field, spin–orbit coupling, and low-symmetry strain contributions to the energy respectively.

2.2.1. E⊗e Vibronic Hamiltonian. In the following formulation of the E⊗e Jahn–Teller Hamiltonian, we make use of the so-called "cluster model",[15] where we consider coupling of the E orbital state to a single pair of distortion coordinates, Q_x and Q_y, representing the appropriate modes of distortion of the Jahn–Teller ion and its nearest neighbors.

The matrices of the E⊗e vibronic Hamiltonian are traditionally expressed in terms of the cubic $|\theta\rangle,|\varepsilon\rangle$ orbital basis, and the explicit form of the Jahn–Teller matrices in these bases is given elsewhere.[1,16,17] In the present article, however, we present the matrices in the complex-trigonal orbital basis. This basis is a natural choice for the construction of the effective Hamiltonian matrix in section 3. With respect to the $|u_+\rangle,|u_-\rangle$ orbital basis, the vibronic Hamiltonian, correct to second order, has the following form,

$$H_{JT} = A_1\begin{pmatrix} 0 & Q_x + iQ_y \\ Q_x - iQ_y & 0 \end{pmatrix} + A_2 \begin{pmatrix} 0 & {Q_y}^2 - {Q_x}^2 + 2iQ_xQ_y \\ {Q_y}^2 - {Q_x}^2 - 2iQ_xQ_y & 0 \end{pmatrix} \tag{5}$$

$$H_{ph} = \frac{1}{2}\begin{pmatrix} ({P_x}^2 + {P_y}^2 + {Q_x}^2 + {Q_y}^2)\hbar\omega & 0 \\ 0 & ({P_x}^2 + {P_y}^2 + {Q_x}^2 + {Q_y}^2)\hbar\omega \end{pmatrix} \tag{6}$$

where Q_x and Q_y are the components of the degenerate $\nu_2(ML_6)$ stretching vibration, transforming as the two components of the e irreducible representation in a trigonal point group. Displacements along these coordinates may be expressed in a basis of increments in the metal–ligand (M-L) bond lengths:

$$Q_x = \frac{1}{\sqrt{12}}(2r_1 + 2r_4 - r_2 - r_5 - r_3 - r_6)$$

$$Q_y = \frac{1}{2}(r_2 + r_5 - r_3 - r_6) \tag{7}$$

where r_i is a unit displacement along the M-L_i bond vector and the ligands are numbered according to the scheme used in Figure 1.

A_1 and A_2 are the first-order and second-order Jahn–Teller coupling constants and $\hbar\omega$ is the energy of the vibration. H_{ph} is the Hamiltonian for an e phonon mode before coupling, and Q_i and P_i are dimensionless operators, related to the observables for position and momentum, q_i, p_i by,

$$Q_i = \sqrt{\frac{\mu\omega}{\hbar}}q_i, \quad P_i = \frac{1}{\sqrt{\mu\hbar\omega}}p_i \tag{8}$$

where μ is the reduced mass of the phonon mode. The unit displacements, r_i are related to q_x and q_y by,

$$r_1 = r_4 = \frac{1}{\sqrt{12}}2q_x; \quad r_2 = r_5 = \frac{(-q_x + \sqrt{3}q_y)}{\sqrt{12}}; \quad r_3 = r_6 = \frac{(-q_x - \sqrt{3}q_y)}{\sqrt{12}} \tag{9}$$

Finally, H_{st} has the following form in the E orbital basis.

$$H_{st} = \begin{pmatrix} 0 & e_x + ie_y \\ e_x - ie_y & 0 \end{pmatrix} \tag{10}$$

where e_x and e_y are the two components of low-symmetry strain, having the same transformation properties as Q_x and Q_y above.

2.2.2. Potential-Energy Surfaces Resulting from E⊗e Jahn–Teller Coupling. In the adiabatic approximation, in which the kinetic contribution to the energies is neglected, diagonalization of the Jahn–Teller matrices defined in eqs 5 and 6 yields analytical expressions for the two adiabatic potential-energy sheets (APES) as functions of the Q_x and Q_y distortion coordinates. In Figure 2 are presented plots of the two APES, calculated using the parameters $A_1 = -900$, $A_2 = 0$, and $\hbar\omega = 254$ cm^{-1}.

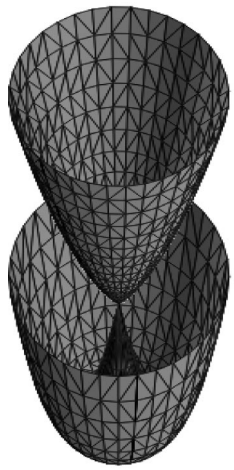

Figure 2. 3D-plots of the two APES resulting from first-order Jahn–Teller coupling.

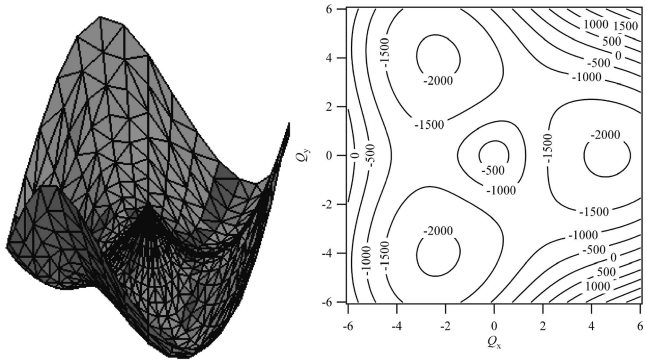

Figure 3. 3D and contour plots of the lower APES resulting from first-order and second-order Jahn–Teller coupling. Energies are given in wavenumbers.

The lower potential-energy surface has the form of a "Mexican hat" and the difference in the energies between the two potential-energy surfaces at distortion coordinates at the bottom of the trough is $4E_{JT}$, where E_{JT} is the Jahn–Teller stabilization energy, defined as $E_{JT} = A_1^2/2\hbar\omega$. The vibronic structure resulting from diagonalization of the full vibronic Hamiltonian exhibits a particularly large density of states at $\sim 4E_{JT}$ above the ground state. Optical transitions observed between the ground-state and these excited states are therefore helpful in obtaining estimates for E_{JT} and consequently for the first-order Jahn–Teller coupling constant, A_1. In the framework of the ligand-field model the observed spectral band is commonly assigned to the d−d transition between the $^{2S+1}B_{1g}$ and $^{2S+1}A_{1g}$ (D_{4h}) terms.

When, in addition to first-order coupling, second-order coupling is also considered, warping of the lower potential-energy surface occurs, resulting in an undulating variation of the potential energy along the bottom of the trough. In Figure 3 are presented 3D and contour plots of the lower APES, calculated using the parameters $A_1 = -900$, $A_2 = 30$ cm^{-1}, and $\hbar\omega = 254$ cm^{-1}. These are the parameters employed to model the data of $[Cr(OD_2)_6]^{2+}$ in the Tutton's salts.[1] If the undistorted geometry has O_h point symmetry, the resulting three potential minima and three maxima in the trough are at distortion coordinates corresponding to special points of D_{4h} cokernel symmetry. All other points

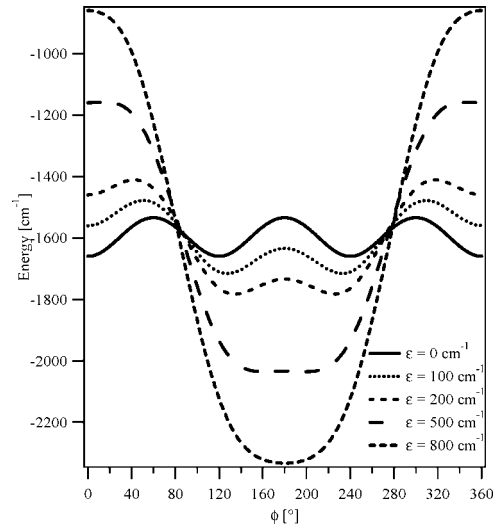

Figure 4. Plots along the path of minimum potential energy of the lowest APES as a function of ϕ, calculated for various strain magnitudes, ε.

on the potential-energy surface correspond to geometries of D_{2h} kernel symmetry. Alternatively, if the original undistorted geometry has S_6 symmetry, any distortion in the $\{Q_x, Q_y\}$ coordinate space will correspond to a lowering of symmetry to C_i symmetry. Defining a position in $\{Q_x, Q_y\}$ coordinate space in terms of the polar coordinates $\{\rho, \phi\}$ such that $Q_x = \rho \cos \phi$ and $Q_y = \rho \sin \phi$, the turning points of the lower potential-energy surface are

$$\rho = \frac{\pm A_1}{\hbar\omega \pm (-1)^n 2A_2}, \quad \phi = \frac{n\pi}{3},\ n = 0, 1, ..., 5 \qquad (11)$$

assuming that $\hbar\omega$ is larger than A_2. The upper and lower signs correspond to the cases $A_1 > 0$ and $A_1 < 0$ respectively. If $A_1/A_2 < 0$, the minima points occur for $n = 0$, 2, 4 and saddle-points for $n = 1$, 3, 5, while for the case $A_1/A_2 > 0$, the two types of points are interchanged.[18] In accordance with our definitions of Q_x and Q_y above, turning points occurring at $\phi = 0$, $2\pi/3$, and $4\pi/3$ correspond to tetragonally-elongated geometries, whereas those occurring at $\phi = \pi/3$, π, and $5\pi/3$ equate to tetragonally-compressed geometries.

Analytical expressions for the lowest APES, resulting from first-order and second-order Jahn–Teller coupling and low-symmetry strain, can be obtained by diagonalization of (5), (6), and (10), where the terms in P are once again ignored. If we express the components of strain in terms of the strain magnitude, ε, and strain angle, θ, such that $e_x = -\varepsilon \cos \theta$ and $e_y = -\varepsilon \sin \theta$, the effect of strain on the form of the APES is easily rationalized. Using this scheme, in the limit where $A_2 = 0$, the effect of strain is to create one potential minimum at $\{Q_x, Q_y\}$ distortion coordinates corresponding to $\phi = \theta$ with a depth of 2ε. In Figure 4 are presented plots along the path of minimum potential energy as a function of ϕ for various ε. The lowest APES was calculated using the parameters: $A_1 = -900$, $A_2 = 5$, $\hbar\omega = 254$, $e_x = \varepsilon$ and $e_y = 0$ cm^{-1}. This particularly simple choice of parameters, corresponding to $\theta = \pi$, shows the effect of strain on the APES very clearly.

In the limit $A_2/\varepsilon \rightarrow 0$, the minimum of the potential-energy surface is determined by the components of strain

and for $\varepsilon = 800$ cm^{-1} and $\theta = \pi$ is found at $\{Q_x, Q_y\}$ coordinates corresponding to $\phi = \pi$ and hence to a tetragonal compression. When $\varepsilon = 0$, the minima of the potential-energy surface are determined completely by A_2 and are at $\{Q_x, Q_y\}$ coordinates corresponding to $\phi = 0$, $2\pi/3$, and $4\pi/3$ and thus to tetragonal elongations. In the intermediate regime, the form of the potential-energy surface is dictated by the relative magnitudes of the A_2 and ε parameters. In our example, as ε is increased, the positions of the potential minima are distorted more and more toward $\{Q_x, Q_y\}$ coordinates corresponding to $\phi = \pi$.

In the limit of infinitely large nuclear masses, i.e., for infinitely small phonon energies, we expect the equilibrium configuration of the complex to correspond to the minimum of the potential-energy surface. While in reality this condition is never met, if ε or A_2 are large compared to the thermal or phonon energies, the distortion coordinates at the minimum of the potential-energy surface will yield a reasonable first approximation of the molecular geometry. If ε or A_2 are comparable in magnitude to the thermal energies a dependence of the observed molecular geometry on the temperature is expected. In this case, a more accurate calculation of the molecular geometry can be obtained by solving the full vibronic Hamiltonian. Once the eigenvalues and eigenvectors have been obtained, the geometry can be determined from the expectation values of the Q_x and Q_y operators in the thermally occupied vibronic states, using eqs 8 and 9.[1]

2.2.3. ^{5}E⊗e Vibronic Hamiltonian. In the case of d^1 and d^9 systems, an extension of the E⊗e vibronic Hamiltonian to include spin is relatively straightforward. These systems are uncomplicated by the effects of electron repulsion, and the small basis size, only ten electronic states, means that H_{el} can be explicitly included in the calculations. By contrast, the d^4 electronic configuration gives rise to a total of 210 electronic states. The sheer magnitude of the resulting vibronic-coupling matrix renders an explicit treatment of H_{el} impractical. Instead, the effects of H_{el} on the energies of the ^{5}E ground term are absorbed into an effective Hamiltonian, constructed using second-order perturbation theory.

The temperature dependence of crystallographic and inelastic-neutron-scattering (INS) data for the $(ND_4)_2Cr(OD_2)_6(SO_4)_2$ salt was interpreted previously in terms of a ^{5}E⊗e vibronic Hamiltonian, perturbed by low-symmetry strain.[1] The electronic part of the Hamiltonian, H_{el}, was accounted for by means of an effective ^5E_g (O_h) Hamiltonian,

$$H_{\text{eff}} = \frac{b}{2}\begin{pmatrix} S_\theta & -S_\varepsilon \\ -S_\varepsilon & -S_\theta \end{pmatrix} \tag{12}$$

expressed in the cubic $|\theta\rangle,|\varepsilon\rangle$ orbital basis, where,

$$S_\theta = S_z^2 - \frac{1}{3}S(S+1); \quad S_\varepsilon = \frac{1}{\sqrt{3}}(S_x^2 - S_y^2) \tag{13}$$

and S_x, S_y, and S_z are the spin-angular-momentum operators operating in the basis of the $S = 2$ spin states.[1,19] The effective-Hamiltonian parameter, b, describes the perturbation of the ^{5}E ground term through spin–orbit coupling, and an approximate expression for this parameter in terms of the spin–orbit-coupling, cubic-field, and electron-repulsion parameters was derived explicitly using second-order perturbation theory by Weihe and Mossin.[16]

A more general effective ^{5}E (C_{3v}) Hamiltonian was presented previously by Simpson et al.[20] This Hamiltonian is also applicable to D_{3d}, D_{3h}, S_6, and O_h symmetries and, given in the complex-trigonal $|u_+\rangle,|u_-\rangle$ orbital basis, has the following general form,

$$H_{\text{eff}} = \begin{pmatrix} \lambda S_z + dS_z^2 & \frac{\mu_1}{2}(S_+S_z + S_zS_+) + \mu_2 S_-^2 \\ \frac{\mu_1}{2}(S_-S_z + S_zS_-) + \mu_2 S_+^2 & -\lambda S_z + dS_z^2 \end{pmatrix} \tag{14}$$

where S_-, S_+, and S_z are the spin-angular-momentum operators operating in the basis of the $S = 2$ spin functions, and λ, d, μ_1, and μ_2 are the effective-Hamiltonian parameters. In perfect cubic symmetry, the effective ^{5}E Hamiltonian reduces to a particularly simple form. In this instance $\mu_1 = 2\sqrt{2}\mu_2$ and $d = \lambda = 0$. Making the substitution $\mu_2 = b/6$, the energies of the ^{5}E spinor levels are then $-2b$, $-b$, 0, b, and $2b$. The result is an effective cubic ^{5}E Hamiltonian, expressed in the complex-trigonal basis.

2.2.4. Ham Theory. The E⊗e Jahn–Teller interaction, operating within a $^{2S+1}$E electronic ground term, gives rise to a $^{2S+1}$E vibronic ground term. In the case of first-order Jahn–Teller coupling the first excited levels are accidentally degenerate vibronic $^{2S+1}A_1$ and $^{2S+1}A_2$ singlet levels. When second-order Jahn–Teller coupling is included, the pseudo-degeneracy of the excited vibronic singlets is lifted. As the magnitude of second-order coupling is increased, the $^{2S+1}$E vibronic ground term is approached asymptotically by either the $^{2S+1}A_1$ or $^{2S+1}A_2$ excited vibronic singlet term. The difference in the energies of the lower-lying doublet and the first excited singlet is referred to in the literature as the tunnelling splitting, 3Γ, and depends inversely on the strength of the vibronic coupling.

Ham derived a generalized matrix form for interactions which may perturb a vibronic $^{2S+1}$E ground term and the next excited orbital-singlet level, resulting from strong first-order and second-order Jahn–Teller coupling.[21] When the lowest excited orbital-singlet state is close in energy to the ground state, we must include it in setting up the secular equation for the effect of any perturbation on the ground state. In the case where the excited singlet is of symmetry A_1, this matrix has the following form with respect to the basis states $|A_1\rangle$, $|g\theta\rangle$, and $|g\varepsilon\rangle$,

$$H = \begin{pmatrix} 3\Gamma & rG_\theta & rG_\varepsilon \\ rG_\theta & -qG_\theta & qG_\varepsilon \\ rG_\varepsilon & qG_\varepsilon & qG_\theta \end{pmatrix} \tag{15}$$

where $|g\theta\rangle$ and $|g\varepsilon\rangle$ are the two components of the E vibronic ground term, which transform as the θ and ε components of the E representation. The corresponding matrix for $|A_2\rangle$ lower is

$$H = \begin{pmatrix} 3\Gamma & rG_\varepsilon & -rG_\theta \\ rG_\varepsilon & -qG_\theta & qG_\varepsilon \\ -rG_\theta & qG_\varepsilon & qG_\theta \end{pmatrix} \tag{16}$$

In the above matrices q and r are the Ham reduction factors. For zero vibronic coupling, $q = 1$ and $r = 0$; for strong first-order Jahn–Teller coupling, $q = -r = {}^1/_2$; and for strong first-order and appreciable second-order coupling, $q = -r/\sqrt{2} = {}^1/_2$. The operators G_θ and G_ε are functions of the relevant perturbations which transform as the θ and ε components of the E representation in cubic symmetry. The effective spin–orbit-coupling matrix is generated by making the following substitutions: $G_\theta = -b/2S_\theta$ and $G_\varepsilon = -b/2S_\varepsilon$ where S_θ and S_ε are the operators defined in eq 13 above, operating in a basis of the spin functions. The corresponding substitutions required to generate the strain matrix are: $G_\theta = e_\theta$ and $G_\varepsilon = e_\varepsilon$, where e_θ and e_ε are the tetragonal and rhombic strain parameters, respectively.

In the limit of weak first-order Jahn–Teller coupling, where the energy separation between the $^{2S+1}$E vibronic ground term and excited vibronic-singlet terms is large relative to the magnitude of an applied perturbation, the effect of Jahn–Teller coupling on the ground term is simply to reduce the parameter entering the description of the perturbation. The following example shall serve to illustrate.

By replacing the operators G_θ and G_ε in eq 15 above with the expressions corresponding to the spin–orbit interaction, an effective spin–orbit-coupling matrix, operating in the ^{5}E and excited ^{5}A$_1$ vibronic bases, can be constructed. In the limit where $3\Gamma >> b$, we can neglect the off-diagonal matrix elements between the ^{5}E vibronic ground term and excited singlets. Expanding the $|g\theta\rangle,|g\varepsilon\rangle$ part of the matrix in eq 15 into a basis consisting of product functions of the vibronic states and the five $S = 2$ spin states, the eigenvalues of the matrix are $-2qb$, $-qb$, 0, qb, and $2qb$. When $q = 1$, the matrix is identical to the ^{5}E effective-Hamiltonian matrix given in eqs 12 and 13, and the eigenvalues correspond to the energies of the spinor levels of the uncoupled ^{5}E electronic ground term. The effect of Jahn–Teller coupling on the spinor energies of the ^{5}E ground term is then to replace the parameter b by $b' = qb$ resulting in a uniform reduction in the energies.

3. ^{3}T$_1$ + (^{5}E⊗e) Vibronic Hamiltonian

In all of the Jahn–Teller-coupling calculations carried out thus far to model the electronic and molecular structures of high-spin d^4 complexes a ^{5}E effective Hamiltonian has been employed. The effects of spin–orbit coupling and the trigonal-splitting of higher-lying terms have been included only insofar as they are allowed to perturb the energies of the ^{5}E basis functions. Such an approach takes no account of the contamination of these functions through the in-mixing of higher-lying states. In particular, when these states are close in energy compared to the magnitude of spin–orbit coupling, the zeroth-order wave functions are no longer a good approximation to the ground state, and perturbation theory breaks down. As we will later see, a contamination of the wave functions has a profound effect on the degree of quenching of the electronic operators within the ^{5}E ground term.

We present here a new ^{3}T$_1$ + (^{5}E⊗e) vibronic-coupling model, where the effective Hamiltonian is extended to span both the ^{5}E and excited ^{3}T$_1$ bases. The matrix elements of spin–orbit coupling between the ^{5}E and ^{3}T$_1$ terms, and the trigonal splitting of the ^{3}T$_1$ term are included explicitly. Spin–orbit coupling to higher-lying terms is still treated as a second-order perturbation on the ^{5}E part of the electronic basis only. The general form of the ^{5}E part of the electronic Hamiltonian in the complex-trigonal basis is given in eq 14. The form of the ^{3}T$_1$ part of the matrix and of the off-diagonal spin–orbit-coupling matrix between the ^{5}E and ^{3}T$_1$ terms has been presented elsewhere.[22,23]

The explicit form of the effective Hamiltonian for a given set of ligand-field parameters can be derived from the d^4 ligand-field matrices. Here, we parametrize the ligand field in terms of the AOM, where the d-orbital energies are expressed in terms of the metal–ligand σ- and π-bonding parameters, e_σ, $e_{\pi\|}$, and $e_{\pi\perp}$. This model provides an obvious link between the d-orbital energies and the structure of the complex. The pictorial simplicity of the AOM approach and transferability of the AOM parameters from one complex to another confer obvious advantages over the crystal-field approach.

We shall now outline the procedure for constructing the effective Hamiltonian from the AOM matrices. First, the ligand-field, spin–orbit coupling, spin- and orbital-angular-momentum matrices are constructed in the full d^4 electronic basis, using the program LIGFIELD.[24] For a given set of AOM and Racah parameters the ligand-field and electron-repulsion matrices are diagonalized together. The nineteen lowest-lying states then correspond to the ^{5}E and ^{3}T$_1$ terms, and the eigenfunctions are now used to transform the Hamiltonian matrices into this new "ligand field" basis.

We require that the orbital components of the ^{5}E basis functions transform as $|u_+\rangle$ and $|u_-\rangle$. In trigonal symmetry, this is easily achieved by diagonalization of the matrix representation of L_z within this term. However, in the special case of perfect octahedral geometry, the operator L_z has no nonzero matrix elements within the ^{5}E ground term. To facilitate the identification of the orbital states, we perturb the AOM input geometry away from perfect octahedral symmetry by introducing a very small trigonal distortion. With a little additional effort, ^{5}E and ^{3}T$_1$ basis functions that are eigenfunctions of both the L_z and S_z operators can be created. This is accomplished by the diagonalization of the matrix representation of the operator: $L_z + S_z$ operating only within the ^{5}E and ^{3}T$_1$ terms.

As the Jahn–Teller and strain matrices have been constructed separately, the relative phases of the resulting ^{5}E basis functions do matter here. From the table of Clebsch−Gordan coefficients for trigonal bases,[25] we can construct the following operator equivalents, transforming as the u$_+$ and u$_-$ components of the E irreducible representation,

$$O_{Eu_+} = \frac{1}{2}(L_x^2 - L_y^2 - i(L_xL_y + L_yL_x))$$
$$O_{Eu_-} = \frac{1}{2}(L_y^2 - L_x^2 - i(L_xL_y + L_yL_x)) \qquad (17)$$

In the complex-trigonal $|u_+\rangle,|u_-\rangle$ orbital basis, the matrices of these operators must have the following form,

$$O_{Eu_+} = \begin{pmatrix} 0 & -1 \\ 0 & 0 \end{pmatrix}, \quad O_{Eu_-} = \begin{pmatrix} 0 & 0 \\ +1 & 0 \end{pmatrix} \qquad (18)$$

Following inspection of the form of the matrices of these operators and of the S_+ operator in a basis of the new ^5E functions, the phases of the eigenfunctions are corrected accordingly. Finally these functions are used to transform the ligand-field and spin–orbit-coupling matrices into the new basis.

Having now obtained the numerical ligand-field and spin–orbit-coupling matrices in an appropriate basis, we calculate the matrix elements of the spin–orbit perturbation, V on the ^5E part of the basis according to the prescription,

$$\langle i|V|j\rangle = \sum_{n=20}^{210} \frac{\langle i|H_{SO}|n\rangle\langle n|H_{SO}|j\rangle}{E_i - E_n} \tag{19}$$

The indices i,j refer to the states belonging to the ^5E term; the index n runs over all 210 ligand-field states resulting from the d^4 electronic configuration, excepting the states belonging to the ground ^5E and $^3T_1$ states; and E_i and E_n are the energies of the ligand-field states resulting from diagonalization of the ligand-field and electron-repulsion matrices. The resulting perturbation, V, has the general matrix form given in eq 14 above. Finally, the complete effective Hamiltonian in the new $^3T_1 + {}^5E$ basis is constructed according to,

$$H_{eff} = V + H_{SO} + H_{LF} + H_{ER} \tag{20}$$

where H_{SO} includes the matrix elements of spin–orbit coupling within and between the ^5E and $^3T_1$ terms, not accounted for in the perturbation. In this basis $H_{LF} + H_{ER}$ is diagonal, corresponding to the energies of the terms before spin–orbit coupling.

The matrix of the $^3T_1 + (^5E\otimes e)$ vibronic Hamiltonian can now be constructed from eqs 5, 6, and 10 and from the effective $^3T_1 + {}^5E$ Hamiltonian, derived from the AOM matrices, in a basis of products of the electronic states and the states of the $\{Q_x, Q_y\}$ harmonic oscillator. A typical calculation with $n_v = 30$ results in a sparse matrix of dimension 9424.

4. Calculations and Discussion

In the following sections, we present example calculations for a variety of Jahn–Teller-coupling strengths, employing the $^3T_1 + (^5E\otimes e)$ model. The results are compared with those obtained using other models, and the dependence of the electronic and molecular structures on the parameters of the vibronic Hamiltonian is discussed.

4.1. First-Order Jahn–Teller Coupling. The three-state model of Ham constitutes a reasonable approximation to the Jahn–Teller Hamiltonian in the limit where spin–orbit coupling and low-symmetry-strain contributions to the Hamiltonian are small compared to Jahn–Teller coupling. Until now, however, no-one has tested the validity of this model by direct comparison of the results with those obtained by solution of the full $^5E\otimes e$ vibronic Hamiltonian. In addition, effects arising from a contamination of the ^5E wave functions by coupling to higher-lying electronic terms have been completely neglected.

In this section, we examine the degree of quenching of the spin–orbit coupling operator within the ^5E ground term

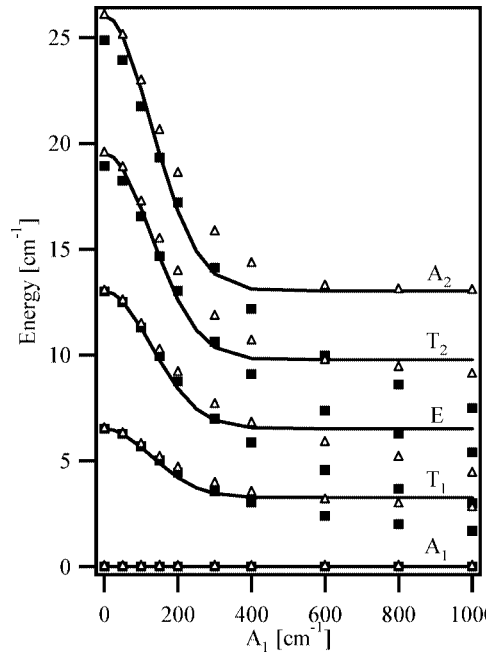

Figure 5. Plots of the ^5E spinor energies as a function of A_1. Solid lines indicate the energies obtained from Ham theory. Open triangles and full squares denote the energies obtained by diagonalization of the $^5E\otimes e$ and $^3T_1 + (^5E\otimes e)$ vibronic Hamiltonians respectively.

for various strengths of first-order Jahn–Teller coupling. We compare and discuss the results of calculations made using both the $^5E\otimes e$ and $^3T_1 + (^5E\otimes e)$ coupling models with those predicted in accordance with the theory of Ham. In Figure 5 are presented plots of the energies of the spinor levels of the ^5E ground term as a function of increasing A_1, calculated using the three approaches.

The full squares show the energies calculated by numerical solution of the $^3T_1 + (^5E\otimes e)$ vibronic Hamiltonian. The effective $^3T_1 + {}^5E$ Hamiltonian was constructed from the AOM matrices, assuming octahedral geometry, with $e_\sigma = 4000$, $e_{\pi\perp} = e_{\pi\parallel} = 0$, $B = 647$, $C = 2640$, and $\zeta = 193.2$ cm^{-1} in accordance with the procedure described in section 3 above. The vibronic Hamiltonian was solved for $\hbar\omega = 254$, $A_2 = 0$, $e_x = e_y = 0$ cm^{-1}, and $n_v = 30$. The ligand-field parameters and phonon energy used are those employed previously to model the EPR and neutron-scattering data of the deuteriated Cr(II) Tutton's salt.[1]

The open triangles show the energies calculated by numerical solution of the $^5E\otimes e$ vibronic Hamiltonian, assuming an effective-Hamiltonian parameter, $b = 6.51$ cm^{-1}. The latter is simply the energy of the first spinor level of the $^3T_1 + {}^5E$ Hamiltonian. Superimposed on this graph are plots of the energies of the spinor levels given by the expressions: $E = -2qb$, $-qb$, 0, qb, and $2qb$. Ham's reduction factor, q, was calculated using the relation,[19]

$$q = \frac{1}{2}[1 + e^{-4E_{JT}/\hbar\omega}] \tag{21}$$

The Mulliken symbols A_1, A_2, E, T_1, and T_2 denote the symmetry and degeneracy of the spinor levels.

For low values of A_1, up to ~100 cm^{-1}, the energies obtained from diagonalization of the full $^5E\otimes e$ vibronic

Hamiltonian agree very well with the predictions of Ham. In the range $A_1 = 200–400\ cm^{-1}$ the reduction factor q is too small. As A_1 is increased, the relative energies of the spinor levels begin to deviate from the pattern, 0, b', $2b'$, $3b'$, $4b'$, deviating most strongly at $A_1 = 1000\ cm^{-1}$ where the excited $^5A_1$ and $^5A_2$ levels are only $\sim 20\ cm^{-1}$ above the ground state. The excited $^5A_1$ and $^5A_2$ terms give rise to spinor levels of E and T_2, and E and T_1 symmetry, respectively. If the excited vibronic-singlet terms are close in energy to the ground vibronic doublet, mixing of spinor levels of the same symmetry occurs, resulting in deviations of the energies of the E, T_1, and T_2 levels from the expected energy scheme. Ham's expression nevertheless gives a surprisingly good reproduction of the energies over the entire range.

Similarly, for low values of A_1, the energies obtained from diagonalization of the $^3T_1 + (^5E\otimes e)$ vibronic Hamiltonian are well approximated by Ham theory. A reasonable reproduction of the energies is achieved for $A_1 < 300\ cm^{-1}$; however, for large values of A_1, the energies calculated from Ham theory are considerably higher than those obtained using the vibronic Hamiltonian. The dominant contribution to the zfs of the ^5E term arises from off-diagonal matrix elements linking the $^3T_1$ and ^5E electronic terms. Though the form of the off-diagonal spin–orbit-coupling matrix between the ^5E vibronic ground term and the electronic $^3T_1$ term must from symmetry be the same as that of the matrix connecting the original ^5E and $^3T_1$ electronic terms, the factor reducing these off-diagonal matrices does not need to be identical to the factor q reducing the operators within the ^5E term. Indeed, in the strong-coupling limit, the effective reduction factor is far smaller than the factor $q = {}^1/_2$, predicted by Ham theory.

4.1.2. Reduction Factors and Ligand-Field Theory. In the limit of weak first-order Jahn–Teller coupling, the low-level energy schemes, calculated above, can also be reproduced using a crystal-field or ligand-field model, with a reduced spin–orbit-coupling parameter. From Ham's reduction factor, $q = 0.5$ for strong first-order Jahn–Teller coupling, the effective spin–orbit-coupling parameter, ζ', required to model the low-level energy scheme with a ligand-field model is calculated to be $\zeta' = \sqrt{0.5}\zeta \simeq 0.707\zeta$. In contrast, the energies obtained using the $^3T_1 + (^5E\otimes e)$ vibronic Hamiltonian, with $A_1 = 1000\ cm^{-1}$, correspond to $q = 0.3$ and an effective spin–orbit-coupling parameter, $\zeta' = \sqrt{0.3}\zeta \simeq 0.55\zeta$. This reduction of the spin–orbit-coupling parameter is much greater than the usual reductions applied to the electronic-repulsion and spin–orbit-coupling parameters, attributed to the effects of covalency.[26]

In the case of strong first-order Jahn–Teller coupling, the higher-lying singlet terms are close in energy to the ground orbital doublet and the spinor energy-level scheme differs significantly from the regular spacing expected from ligand-field theory. In addition, the observation of an optical transition of energy $\sim 4E_{JT}$, typical for first-order Jahn–Teller coupling, cannot be reconciled with a perturbed ^5E ground term within the ligand-field model.

4.2. Strong First-Order and Weak Second-Order Jahn–Teller Coupling. Acoustic paramagnetic resonance (APR), far-infrared (FIR), phonon-scattering, and thermal-conductivity experiments have been carried out on MgO:Cr^{2+}, $KMgF_3$:Cr^{2+}, and CaO:Cr^{2+}.[27–34] In these hosts, the chromous ion is embedded substitutionally for Mg^{2+} or Ca^{2+} at a site of approximately cubic symmetry and is very strongly coupled to the lattice vibrations. The energy splittings observed in these systems can be interpreted with the aid of Ham's three-state model, assuming strong first-order and weak second-order Jahn–Teller coupling with very small lattice strain.

The magnitude of the tunnelling splitting in the MgO:Cr^{2+} system is of the order of $\sim 10–30\ cm^{-1}$.[35] The degeneracies of the ^5E ground term and the excited $^5A_1$ and $^5A_2$ terms, arising from Jahn–Teller coupling, are then lifted through the spin–orbit interaction. Although a considerable amount of data has been amassed for the MgO:Cr^{2+} system, a number of different parameter sets have been proposed.[32,36,37] In the following, we do not attempt to model the data for this system. Instead these calculations should serve to illustrate, qualitatively, the energy scheme resulting from strong first-order and weak second-order Jahn–Teller coupling, as observed in such systems.

In Figure 6 are presented plots of the energies of the lowest fifteen spinor levels of a representative high-spin d^4 cation as a function of ζ, calculated by diagonalization of (a) the $^5E\otimes e$ vibronic Hamiltonian and (b) the $^3T_1 + (^5E\otimes e)$ vibronic Hamiltonian. The effective $^3T_1 + {}^5E$ Hamiltonian was created from the AOM matrices, assuming octahedral coordination. The ligand-field parameters were those used to construct the matrices in section 4.1. The effective-Hamiltonian parameter, b, is directly proportional to ζ^2, and an expression for this parameter was derived from the spinor energies of the $^3T_1 + {}^5E$ Hamiltonian. In both calculations, the parameters $\hbar\omega = 254$, $A_1 = -900$, $A_2 = 1$, $e_x = e_y = 0\ cm^{-1}$, and $n_v = 30$ were used.

Superimposed on these plots are calculations based on Ham's three-state model. Once again, we have constructed the effective spin–orbit-coupling matrix by substituting the relevant functions for the G_θ and G_ε operators. The matrix given in eq 16 above, with $|A_2\rangle$ lower lying was expanded into a new basis consisting of product functions of the three vibronic states and the five $S = 2$ spin states. $3\Gamma = 16.66\ cm^{-1}$ was obtained by numerical solution of the $^5E\otimes e$ vibronic Hamiltonian, without spin–orbit coupling. Finally, the energies were obtained by diagonalization of the resulting matrix, with the parameters $3\Gamma = 16.66\ cm^{-1}$, $q = -r = {}^1/_2$ and b as determined above.

In Figure 6a, the energies calculated using Ham's three-state model are in very good agreement with those obtained from diagonalization of the $^5E\otimes e$ vibronic Hamiltonian. In Figure 6b, however, the spinor energies calculated using Ham's model give poor agreement with the solutions of the $^3T_1 + (^5E\otimes e)$ vibronic Hamiltonian. This is a consequence of an overestimate in the factor q, as already mentioned. This result emphasizes the need for caution when using second-order perturbation theory. While the effective ^5E Hamiltonian may yield reasonable approximations to the energies of the spinor levels when the $^3T_1$ term is relatively high in energy, the Hamiltonian does not allow for any contamination of the ground-state wave functions, which will most certainly

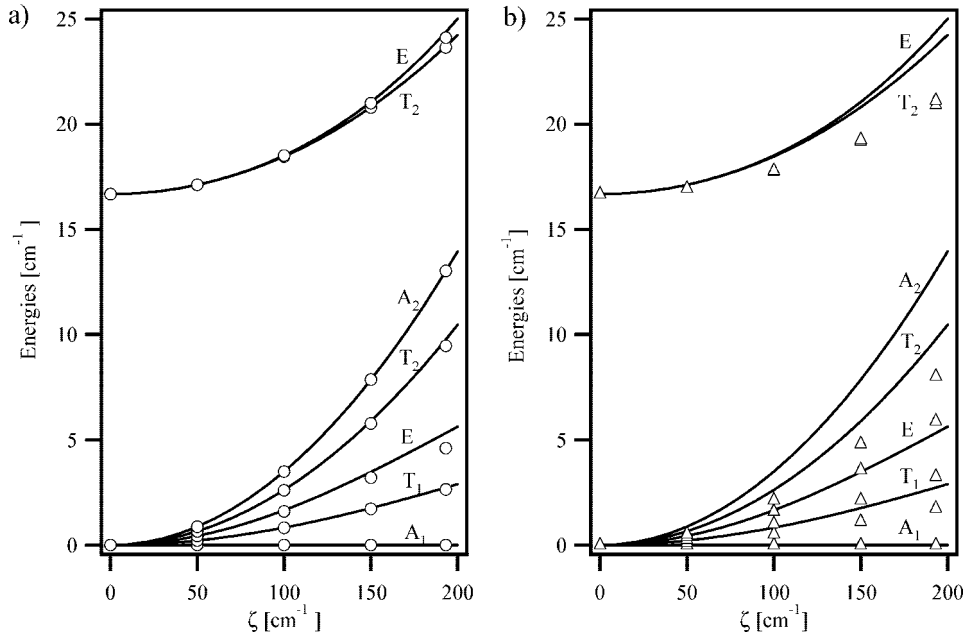

Figure 6. Plots of the lowest fifteen spinor levels as a function of ζ. Lines indicate the energies obtained using Ham theory. Open circles and open triangles denote the energies calculated by diagonalization of the $^5E\otimes e$ vibronic and $^3T_1 + (^5E\otimes e)$ vibronic Hamiltonians, respectively. The parameters used are given in the text.

have an influence on the value of q. In this respect, the effective $^3T_1 + {}^5E$ Hamiltonian must be considered to be more exact.

4.3. Strong First-Order and Appreciable Second-Order Jahn–Teller Coupling. Of the high-spin d^4 centers for which experimental data are known, the instance of strong first-order coupling and very weak second-order coupling, considered in the previous section, is found only for the chromous ion doped into MgO and CaO. The remainder are primarily Mn(III) coordination complexes for which the large ratio of the strain to the tunnelling splitting renders a static Jahn–Teller distortion at liquid-helium temperatures. The ground-state multiplet may then be adequately described by an $S = 2$ spin Hamiltonian.

Correlating the parameter values of this Hamiltonian to the molecular structure traditionally proceeds by ligand-field theory, from which information regarding the bonding within the complex is obtained. Before proceeding further, it is vital to outline the approach and emphasize its limitations. The ligand-field Hamiltonian is often constructed using the AOM. Some dependence of the parameters upon the distance, r, then has to be assumed. In the spirit of crystal-field theory, e_σ and e_π would be assigned a $1/r^5$ and $1/r^6$ dependence, respectively.[2] The values of the bonding parameters so derived then have chemical significance only if the complex is strongly localized in the temperature range where the experimental data are acquired, for dynamic effects cannot be modeled by a Hamiltonian in which the vibrational coordinates of the complex are neglected. For example, room-temperature crystallographic data are often interpreted in conjunction with low-temperature spectroscopic data. This strategy is potentially dangerous since the room-temperature crystal structure often does not reflect the structure of the molecule at base temperature.

If the crystallographic and spectroscopic data are collected at the same temperature but dynamic effects are still prevalent, then the results of the analysis will still be misleading, as the values of the spin-Hamiltonian parameters derived will depend on the time scale of the technique relative to the rate at which the molecule undergoes intramolecular reorientations between the potential-energy minima. By contrast, in the theoretical method which we have outlined, the angular-overlap matrices are constructed in the undistorted geometry and are always valid regardless of the coupling strength. The calculated molecular and electronic coordinates appear naturally from the vibronic-coupling calculations.

As an illustration, we consider here the $[Mn(OD_2)_6]^{3+}$ cation in the deuteriated cesium manganese alum, $CsMn(SO_4)_2\cdot 12D_2O$. Single-crystal neutron-diffraction studies reveal that the site symmetry of the $[Mn(OD_2)_6]^{3+}$ cation in the alum at 170 K is S_6. The water molecules are rotated about the Mn−O bond vectors by the angle $\varphi = -19$ degrees with respect to the MnO_6 framework.[35] At ∼156 K, however, the alum undergoes a cubic to orthorhombic phase transition, and at 5 K, the aqua ion is tetragonally elongated, with Mn−O bond distances of 2.129(2), 1.929(1), and 1.924(1) Å and all O−Mn−O bond angles within 1.4 of 90°.[38]

Despite the MnO_6 framework being close to tetragonal, an analysis of the low-temperature HFEPR data indicates a large rhombic anisotropy, with spin-Hamiltonian parameters $D = -4.491(7)$ cm^{-1} and $E = 0.248(5)$ cm^{-1}.[2] Similar parameters were obtained from 1.5 K INS spectra.[3] The AOM analysis of the low-temperature data has been reported in detail and may be summarized as follows. The optical spectra exhibit intra-^5D transitions, which energies may be written down in terms of AOM bonding parameters. As-

suming parameters corresponding to the $[V(OH_2)_6]^{3+}$ cation, and allowing the e_π parameters to vary as a function of $1/r^6$, it was concluded that the rhombic anisotropy results primarily from the anisotropic nature of the Mn(III)−water π-bonding.

Recently, we have collected data at elevated temperatures showing that the spin-Hamiltonian parameters are temperature dependent. In the spirit of the AOM, this result can be modeled only by allowing the parameters to be temperature dependent, implying that the nature of the bonding interaction is itself temperature dependent. This is not necessarily so. We now show how the low-temperature bond lengths and spin-Hamiltonian parameters can be reproduced by our model and how these experimental observables can become temperature dependent without implying a change in parameters describing the chemical bonding.

4.3.1. Calculation of the Low-Level Energy Structure. Using the $^3T_1 + (^5E\otimes e)$ vibronic Hamiltonian, the low-level energy structure of the Mn(III) aqua ion in the cesium manganese alum can be reproduced. AOM matrices were first constructed using the bond angles of the high-symmetry (S_6) structure and the parameters, $e_\sigma = 6950$, $e_{\pi\perp} = 930$, $e_{\pi\parallel} = 0$, $B = 848$, and $C = 3341$ cm^{-1}, from which an effective $^3T_1 + {}^5E$ Hamiltonian was derived. The Racah parameters are ca. 85% of the free-ion values, and the $e_{\pi\perp}$ and e_σ parameters are those used to model spectroscopic data for the $[V(OH_2)_6]^{3+}$ cation in the cesium vanadium alum.[39]

A band observed at ∼10 500 cm^{-1} in the absorption spectra of the cesium manganese alum corresponds to the intra-^{5}E transition of energy $\sim 4E_{JT}$.[2] An estimate of the energy of the $\nu_2(MnO_6)$ stretching vibration, $\hbar\omega \sim 428$ cm^{-1}, was made based on Raman data available for related systems[40,41] and, using the relation $E_{JT} = A_1^2/2\hbar\omega$, the first-order Jahn–Teller-coupling parameter $A_1 = -1462$ cm^{-1} was obtained. Values of the second-order-coupling and strain parameters were chosen such as to give rise to a sufficiently isolated $S = 2$ ground manifold. Diagonalization of the $^3T_1 + (^5E\otimes e)$ vibronic Hamiltonian using the parameters, $A_1 = -1462$, $A_2 = 30$, $e_x = -100$, $e_y = 0$, $\hbar\omega = 428$ cm^{-1}, $\zeta = 317$ cm^{-1} (ca. 90% of the free-ion value) and $n_v = 35$, yielded a low-level energy scheme characterized by $D = -4.6421$ and $E = 0.2277$ cm^{-1}, in reasonable agreement with the experiment.

4.3.2. Variation in Bond Lengths with Temperature. In addition to calculating the low-level energy structure, it is also possible to calculate the Mn−O bond lengths of the Mn(III) aqua ion. Using the eigenvectors obtained in the calculation above, the expectation values of the Q_x and Q_y operators within the ground multiplet can be determined. From eqs 8 and 9, $\mu = 20$ (the reduced mass of the D_2O ligand) and $\hbar\omega = 428$ cm^{-1}, the distortions r_i of the Mn−O_i bond distances were calculated. Using the average (5 K) Mn−O bond length of 1.994 Å, the resulting Mn−O bond distances are 2.14, 1.93, and 1.93 Å, in very good agreement with the 5 K experimental data.[35]

The solution of the vibronic Hamiltonian described in section 4.3.1 yields two excited spin multiplets at ∼150 cm^{-1} $^3/_2e_x$ above the ground spin multiplet. At room temperature (293 K), the Boltzmann factors for the ground and excited spin multiplets are ∼0.54, ∼0.23, and ∼0.23, respectively. The Mn−O bond distances for the two excited multiplets, calculated from the expectation values of Q_x and Q_y in accordance with eqs 8 and 9, are 1.92, 2.03, and 2.03 Å, corresponding to tetragonally-compressed geometries. An average room temperature structure can be obtained by weighting the geometries of the ground and excited spin multiplets in accordance with their Boltzmann factors. The Mn−O bond distances at 293 K are thus calculated to be 2.03, 1.97, and 1.97 Å. A natural dependence of the bond distances on the temperature is seen to arise without the need to assume a temperature dependence of the parameters of the Hamiltonian.

5. Summary and Conclusion

The theoretical description of high-spin d^4 complexes has traditionally proceeded by way of a conventional ligand-field analysis, correlating spectroscopic data with crystallographic measurements. The approach necessitates assumptions as to the radial dependence of the ligand-field parameters, takes no account of dynamical Jahn–Teller effects, and is of dubious significance when the low-temperature structure of the complex is inferred from room-temperature X-ray diffraction data. In this work, we have presented a new theoretical approach which circumvents these difficulties by calculating the experimental quantities directly from the eigenfunctions and eigenvalues of a vibronic Hamiltonian, yet retains the chemically intuitive AOM in the construction of the electronic basis set.

Whereas the $^5E\otimes e$ vibronic-coupling model is applicable only to certain octahedral Cr(II) complexes, the $^3T_1 + (^5E\otimes e)$ model presented here can in principle be applied to any high-spin d^4 complex, where the ligand-field parameters in the undistorted trigonal or octahedral configuration can be reliably estimated. The utility of the method is demonstrated by the application of the Hamiltonian to $MgO:Cr^{2+}$ and the $[Mn(OD_2)_6]^{3+}$ cation in the deuteriated cesium manganese alum. A temperature dependence of the bond lengths arises quite naturally from the model.

The explicit inclusion of the spin–orbit interaction between the ^5E and excited $^3T_1$ terms has a marked effect on the degree of quenching of spin–orbit coupling within the ground term. For Cr(II) complexes with strong first-order coupling, it is shown that the effective reduction factor is considerably lower than that expected from Ham's theory. This result underlines the need for caution in the interpretation of the ground energy-level scheme observed for systems such as $MgO:Cr^{2+}$.

Acknowledgment. This work was funded by the Swiss National Science Foundation.

References

(1) Dobe, C.; Noble, C.; Carver, G.; Tregenna-Piggott, P. L. W.; McIntyre, G.; Barra, A.-L.; Neels, A.; Janssen, S.; Juranyi, F *J. Am. Chem. Soc.* **2005**, *127* (10), 3642.

(2) Tregenna-Piggott, P. L. W.; Weihe, H.; Barra, A.-L. *Inorg. Chem.* **2003**, *42*, 8504.

(3) Basler, R.; Tregenna-Piggott, P. L. W.; Andres, H.; Dobe, C.; Güdel, H.-U.; Janssen, S.; McIntyre, G. J. *J. Am. Chem. Soc.* **2001**, *123* (14), 3377.

(4) Krzystek, J.; Yeagle, G. J.; Park, J.-H.; Britt, R. D.; Meisel, M. W.; Brunel, L.-C.; Telser, J. *Inorg. Chem.* **2003**, *42*, 4610.

(5) In some instances, fourth order terms may also be required to model the low-level energy scheme. However, these terms are generally very small compared to the terms in *D* and *E*.

(6) Griffiths, J. S. In *The Theory of Transition-Metal Ions*; Cambridge University Press: New York, 1961.

(7) Barra, A.-L.; Gatteschi, D.; Sessoli, R.; Abbati, G. L.; Cornia, A.; Fabretti, A. C.; Uytterhoeven, M. G. *Angew. Chem. Intl. Ed. Engl.* **1997**, *36*, 2329.

(8) Limburg, J.; Vrettos, J. S.; Crabtree, R. H.; Brudvig, G. W.; de Paula, J. C.; Hassan, A.; Barra, A.-L.; Duboc-Toia, C.; Collomb, M.-N *Inorg. Chem.* **2001**, *40*, 1968.

(9) Gerritsen, H. J.; Sabisky, E. S. *Phys. Rev.* **1963**, *132*, 1507.

(10) Telser, J.; Pardi, L. A.; Krzystek, J.; Brunel, L.-C. *Inorg. Chem.* **1998**, *37*, 5769.

(11) Gregson, A. K.; Doddrell, D. M.; Healy, P. C. *Inorg. Chem.* **1978**, *17*, 1216.

(12) Mossin, S.; Weihe, H.; Barra, A.-L. *J. Am. Chem. Soc.* **2002**, *124*, 8764.

(13) Jahn, H. A.; Teller, E. *Proc. Roy. Soc.* **1937**, *A161*, 220.

(14) Englman, R. In *The Jahn-Teller Effect in Molecules and Crystals*; Wiley-Interscience: New York, 1972.

(15) Van Vleck, J. H. *J. Chem. Phys.* **1939**, *7*, 72.

(16) Ham, F. S. *Phys. Rev.* **1968**, *166*, 307.

(17) Dobe, C.; Andres, H.-P.; Tregenna-Piggott, P. L. W.; Mossin, S.; Weihe, H.; Janssen, S. *Chem. Phys. Lett.* **2002**, *362*, 387.

(18) (a) These expressions are similar to those given by Isaac Bersuker in his review of the Jahn−Teller effect; see *Coord. Chem. Rev.* **1975** *14*, 357–412. (b) Note that our formulation of the JT matrices means that the sign in the upper part of the expression for ρ is different, and the relationship between the relative signs of A_1 and A_2 and the positions of the minima are reversed.

(19) Ham, F. S. *J. Phys. Colloq.* **1971**, *32*, 952.

(20) Simpson, J. A. L.; Bates, C. A.; Barrau, J.; Brousseau, M.; Thomas, V. *Semicond. Sci. Technol.* **1988**, *3*, 178.

(21) Ham, F. S. In *Electron Paramagnetic Resonance*; Geschwind, S., Ed.; Plenum Press: New York, 1972; p 45.

(22) Brugel, D.; Bates, C. A. *Semicond. Sci. Technol.* **1987**, *2*, 501.

(23) The matrix elements given in ref 22 relate strictly to Cr^{2+} in tetrahedral coordination. The matrices have, however, the same form for Cr^{2+} in octahedral coordination.

(24) Bendix, J. *Compr. Coord. Chem. II* **2004**, *2*, 673.

(25) Sugano, S.; Tanabe, Y.; Kamimura, H. In *Multiplets of Transition-Metal Ions In Crystals*; Academic Press: New York, 1970.

(26) Figgis, B. N.; Hitchman, M. In *Ligand-Field Theory and Its applications*; Wiley-VCH: New York, 2000.

(27) Marshall, F. G.; Rampton, V. W. *J. Phys. C: Solid State Phys.* **1968**, *1*, 594–598.

(28) Rampton, V. W.; Bates, C. A.; Fletcher, J. R.; Jones, S. C.; Jaussaud, P. C. *Proceedings of the 1st International Conference on Phonon Scattering in Solids*, Paris, 1972; pp 243−246.

(29) Lange, J. N. *Phys. Rev. B* **1973**, *8*, 5999.

(30) Anderson, B. R.; Challis, L. J.; Stoelinga, J. H. M.; Wyder, P. *J. Phys. C: Solid State Phys.* **1974**, *7*, 2234.

(31) King, P. J.; Oates, S. G.; Rampton, V. W.; Shellard, I. J. *Proceedings of the 2nd International Conference on Phonon Scattering in Solids*, Nottingham, 1976; pp 181−183.

(32) Lange, J. N.; Guha, S. *Proceedings of the 2nd International Conference on Phonon Scattering in Solids*, Nottingham, 1976; pp 175−177.

(33) Rampton, V. W.; Shellard, I. J. *Proceedings of the 2nd International Conference on Phonon Scattering in Solids*, Nottingham, 1976; pp 178–180.

(34) Rivallin, J.; Salce, B. *Proceedings of the 2nd International Conference on Phonon Scattering in Solids*, Nottingham, 1976; pp 184–186.

(35) Patel, J. L.; Wigmore, J. K. *J. Phys. C: Solid State Phys.* **1977**, *10*, 1829.

(36) Fletcher, J. R.; Stevens, K. W. H. *J. Phys. C: Solid State Phys.* **1969**, *2*, 444–456.

(37) Ham, F. S. *Phys. Rev.* **1971**, *B4*, 3854.

(38) Tregenna-Piggott, P. L. W.; Andres, H. P.; McIntyre, G. J.; Best, S. P.; Wilson, C. C.; Cowan, J. A. *Inorg. Chem.* **2003**, *42*, 1350.

(39) Tregenna-Piggott, P. L. W.; Spichiger, D.; Carver, G.; Frey, B.; Meier, R.; Weihe, H.; Cowan, J. A.; McIntyre, G. J.; Zahn, G.; Barra, A.-L. *Inorg. Chem.* **2004**, *43* (25), 8049.

(40) Best, S. P.; Beattie, J. K.; Armstrong, R. S. *J. Chem. Soc., Dalton Trans.* **1984**, 2611.

(41) Tregenna-Piggott, P. L. W.; Best, S. P. *Inorg. Chem.* **1996**, *35*, 5730.

CT7003484